

# Tomography of red blood cells by multiple-wavelength digital holographic microscopy

Jonas Kühn,<sup>a</sup> Frédéric Montfort,<sup>b</sup> Tristan Colomb,<sup>b</sup> Benjamin Rappaz,<sup>c</sup> Corinne Moratal,<sup>c</sup> Nicolas Pavillon,<sup>a</sup> Pierre Marquet<sup>c</sup> and Christian Depeursinge<sup>a</sup>

<sup>a</sup>Laboratory of Applied Optics, Ecole polytechnique fédérale de Lausanne (EPFL), CH-1015 Lausanne, Switzerland

<sup>b</sup>Lycée Tec SA, PSE-A, CH-1015 Lausanne, Switzerland

<sup>c</sup>Brain Mind Institute, Ecole Polytechnique Fédérale de Lausanne (EPFL), CH-1015 Lausanne, Switzerland

**Abstract:** We present a method enabling cell tomography by multiple-wavelength digital holographic microscopy. 20 reflection holograms between 485 and 670 nm are sequentially acquired, then the wavefronts are summed to obtain 3D tomographic reconstruction of red blood cells.

© 2009 Optical Society of America

**OCIS codes:** (090.1995) Digital holography; (110.0180) Microscopy; (110.6955) Tomographic imaging

## 1. Multiple-wavelength digital holographic tomography

Digital holographic microscopy (DHM) provides full-field complex objet wavefront retrieval in real-time with an acquisition rate only limited by the camera. Biological applications consists for example in neuron imaging [1], red blood cell analysis [2] or cancerous cell screening [3]. In these experiments, the transmission DHM phase signal is proportional to the integrated optical path length (OPL) through the specimen, dependant on both topology and mean intracellular refractive index. Although methods to decouple both variables exist, the measurement is essentially an integrated value, and no interface or sub-cellular component localization is possible in the  $z$ -direction. Recently, multiple angles digital holographic tomography has been developed in order to retrieve full-3D refractive index map of intra-cellular structures. However all these techniques rely on some mechanical scanning, for instance by rotation of the specimen [4] or change of the illumination beam angle [5].

In our case we use a wavelength-scanned method, thus neither the object nor any part of the setup is mechanically moved. The principle of multiple-wavelength digital holographic tomography [6–8] works as follows: different equally  $k$ -spaced wavelengths full-field holograms are sequentially acquired, and the corresponding wavefronts are summed in order to add constructively in a plane of interest in which they are in phase, and destructively in out-of-plane sections, inducing a slicing effect. Here we present a new approach enabling to detect for the first time the reflection phase signal of fixed red blood cells (RBC), for which the membrane geometry in 3D can be retrieved thanks to the sub-micrometer resolution of the experimental configuration. Our tomography method is a refined version of the one of Ref. 7: when  $N$  back-scattered electric fields  $\Psi_j$  of same amplitude originating from sample point  $P$  at different wavelength  $\lambda_j = 2\pi/k_j$  equally separated by  $\Delta k$  in the  $[k_{min}, k_{max}]$  range are superposed when observed at a point  $Q$ , we obtain the optical sectioning effect along the  $z$ -direction by the filter function  $T(r_{PQ})$  of Eq. 1. This function is also plotted in Fig. 1 for 20 wavelengths in the 485 - 670 nm range.

$$T(r_{PQ}) = \frac{\sin(\Delta k r_{PQ} \frac{N}{2})}{\sin(\Delta k r_{PQ} \frac{1}{2})} \quad (1)$$

with  $r_{PQ} = n_m |\mathbf{r}_P - \mathbf{r}_Q|$  the optical path length (OPL) between  $P$  and  $Q$  in a medium refractive index  $n_m$ .

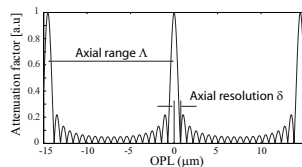


Fig. 1. Nominal Filter Function  $T(r_{PQ})$  for 20 equally  $k$ -spaced wavelengths in the 485-670 nm range.

In addition to this, similarly to the Gaussian function of Ref. 9, we choose to apply a weighting function to reduce the ripples of  $T(r_{PQ})$  in Fig. 1, but in our case we use the Kaiser function of Eq. 2, far more efficient than Gaussian windows when dealing with truncated spectra. We adjusted the  $\alpha$  coefficient to 3.8 to enhance the side lobes suppression from -7 dB to -15 dB, while axial resolution  $\delta$  degrades only to  $\delta = 1 \mu\text{m}$  from 640 nm for the nominal function of Fig. 1.

$$w(k) = \frac{J_0\left(\alpha\sqrt{1 - 4\left(\frac{k}{N\Delta k}\right)^2}\right)}{J_0(\alpha)} \quad (2)$$

with  $\alpha$  being a tunable coefficient between 0 and 10.

## 2. Experimental procedure

The experimental setup is shown in Fig. 2(a), with a femtosecond optical parametric amplifier (OPA) laser source delivering 200-250 fs pulses at 250 kHz, within a 480-675 nm tunable range. Motorized wavelength tuning reaches about 1 nm/s with roughly 1 nm precision and the coherence length ( $L_c$ ) given by the pulse width is about 60-75  $\mu\text{m}$ .

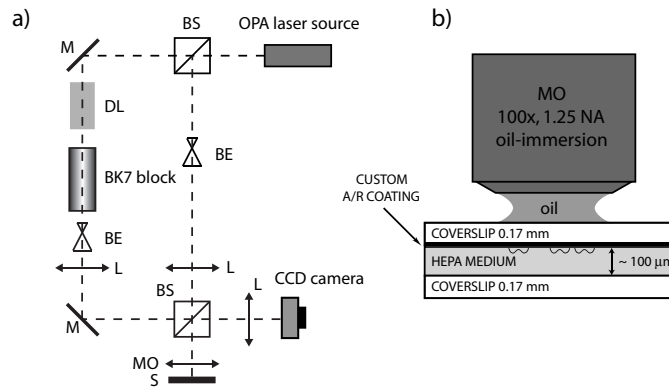


Fig. 2. Experimental arrangement. (a) Optical setup. BS: Beam-splitter, M: Mirror, DL: Delay line, BK7: BK7 glass block, BE: Beam-expander, L: Lens, MO: 1.25 NA 100x oil-immersion microscope objective, S: Specimen. (b) Sample measurement geometry.

The BK7 glass block in the reference arm of Fig. 2(a) permits to compensate for dispersion in the object arm when scanning the wavelength. The sample is a 90% Ethanol-fixed 4  $\mu\text{l}$  blood solution suspended in a HEPA buffer (15 mM HEPES pH 7.4, 130 mM NaCl, 5.4 mM KCl, 10 mM glucose, 1 mM CaCl<sub>2</sub>, 0.5 mM MgCl<sub>2</sub>, and 1 mg/ml bovine serum albumin) sandwiched by two 0.17 mm glass coverslips, as shown in Fig. 2(b), where the glass-sample interface of the upper coverslip is custom-designed with a broadband anti-reflection (A/R) coating reducing glass-water reflectivity to 0.05%. Combined with the inverted geometry, this warrants that the extremely weak signal reflected by the RBC is not lost among the intense glass-water reflection generated at the coverslip interface, as both reflectivities are now ideally in a similar range. This way, direct on-cell phase reflection is now becoming possible, as the preparation thickness far above  $L_c$  ensures that the higher intensity reflection from the lower non-treated coverslip is not contributing to the interference.

Experimentally, the sample is sequentially illuminated by 20 equally  $k$ -spaced wavelengths in the 485-670 nm range, then each complex wavefront is digitally reconstructed. Prior to summation, the different phase offsets  $\varphi_j$  are adjusted for each wavefront in a constant-phase reference plane  $z = 0$ , here the A/R-treated coverslip around the imaged RBC, to avoid random addition [7]. Finally, a phase-only addition is performed as expressed in Eq. 3 for a point  $Q(x, y, z)$ .

$$\Psi(x, y, z) = \sum_{j=0}^{N-1} w_j \frac{\Psi_j(x, y, 0)}{\|\Psi_j(x, y, 0)\|} e^{-i\varphi_j} e^{i\varphi_z} \quad (3)$$

with  $\varphi_z = 4\pi n_m z / \lambda_j$ .

### 3. Results

To the best of our knowledge, Figure 3(a) shows thereafter for the first-time a cellular membrane reflection DHM phase images, an erythrocyte in this case. Then Figure 3(b,c) compares the unitary and the Kaiser-weighted X-Z tomographic cut results on a  $7.5 \mu\text{m}$  axial scale with a slices thickness oversampling of 200 nm.

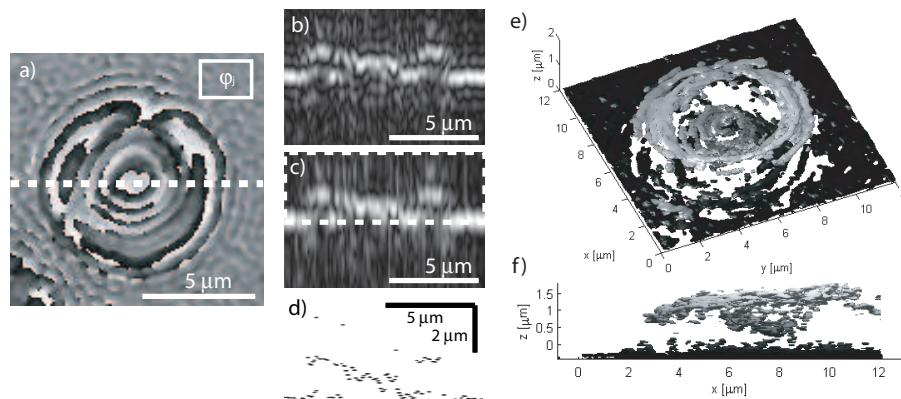


Fig. 3. Tomography of a RBC. (a) Reflection DHM phase image; (b) Tomographic X-Z cut through the cell along the dashed line in (a) with no weighting function; (c) Same as (b) but with  $\alpha = 3.8$  Kaiser weighting function; (d) Peak-detected result applied on a zoomed region (white dashed rectangle) of (c); (e) 3D-representation of the series of peak-detected tomographic cuts as in (d) on the RBC of (a); (f) Lateral view of (e)

When looking at Fig. 3, one can clearly distinguish the surrounding coverslip surface and the well-known biconcave shape of the RBC external membrane, although the height of such cells is only 2-3  $\mu\text{m}$ . Despite the fact that the unitary window reconstruction of Fig. 3(b) may appear sharper, the strong ripples degrades the image interpretation, while the Kaiser cut of Fig. 3(c) is significantly less degraded with little resolution loss. For instance, ripples-free tomographic cuts like the ones of Fig. 3(c) can be used to compute high-resolution cuts with a finer 50 nm slice thickness oversampling as in Fig. 3(d), obtained by a common thresholded local peak-detection algorithm applied along each Z-profiles of the ripples-free Kaiser tomography. Figures 3(e,f) finally show 3D point clouds corresponding to the whole 3D volume resulting from gathering all X-Z cuts like Fig. 3(c).

### 4. Conclusion

The presented multiple-wavelength reflection DHM tomography technique enables submicrometer 3D reconstruction of cells with enough precision to detect the membrane signal, without any mechanical scanning. Such results are promising for interferometric and digital holography investigation of cells or sub-cellular structures, typically for creating models relating the integrated phase signal obtained by these techniques to the volume and true shape of a cell or to investigate of multiple-layer specimen.

### References

1. P. Marquet, B. Rappaz, P. J. Magistretti, E. Cuche, Y. Emery, T. Colomb, and C. Depeursinge, "Digital holographic microscopy: a non-invasive contrast imaging technique allowing quantitative visualization of living cells with subwavelength axial accuracy," *Optics Letters* **30**, 468–470 (2005).
2. B. Rappaz, A. Barbul, Y. Emery, R. Korenstein, C. Depeursinge, P. J. Magistretti, and P. Marquet, "Comparative study of human erythrocytes by digital holographic microscopy, confocal microscopy, and impedance volume analyzer," *Cytometry Part A* **73A**, 895–903 (2008).
3. B. Kemper, D. Carl, J. Schnekenburger, I. Bredebusch, M. Schafer, W. Domschke, and G. von Bally, "Investigation of living pancreas tumor cells by digital holographic microscopy," *Journal of Biomedical Optics* **11**, 034 005 (2006).
4. F. Charrière, A. Marian, F. Montfort, J. Kühn, T. Colomb, E. Cuche, P. Marquet, and C. Depeursinge, "Cell refractive index tomography by digital holographic microscopy," *Optics Letters* **31**, 178–180 (2006).
5. W. Choi, C. Fang-Yen, K. Badizadegan, S. Oh, N. Lue, R. R. Dasari, and M. S. Feld, "Tomographic phase microscopy," *Nature Methods* **4**, 717–719 (2007).
6. M. K. Kim, "Tomographic three-dimensional imaging of a biological specimen using wavelength-scanning digital interference holography," *Optics Express* **7**, 305–310 (2000).
7. F. Montfort, T. Colomb, F. Charrière, J. Kühn, P. Marquet, E. Cuche, S. Herminjard, and C. Depeursinge, "Submicrometer optical tomography by multiple-wavelength digital holographic microscopy," *Applied Optics* **45**, 8209–8217 (2006).
8. M. C. Potcoava and M. K. Kim, "Optical tomography for biomedical applications by digital interference holography," *Measurement Science and Technology* **19**, 074 010 (2008).
9. L. Yu and Z. Chen, "Improved tomographic imaging of wavelength scanning digital holographic microscopy by use of digital spectral shaping," *Optics Express* **15**, 878–886 (2007).